Nano Energy 55 (2019) 164–172

Contents lists available at ScienceDirect

Nano Energy

journal homepage: www.elsevier.com/locate/nanoen

Full paper

Thermodynamic loss mechanisms and strategies for efficient hot-electron photoconversion☆

Cheng Zhang[a,b], Guoyang Cao[a,b], Shaolong Wu[a,b], Weijia Shao[a,b], Vincenzo Giannini[c,d], Stefan A. Maier[c,e], Xiaofeng Li[a,b,*]

[a] School of Optoelectronic Science and Engineering & Collaborative Innovation Center of Suzhou Nano Science and Technology, Soochow University, Suzhou 215006, China
[b] Key Lab of Advanced Optical Manufacturing Technologies of Jiangsu Province & Key Lab of Modern Optical Technologies of Education Ministry of China, Soochow University, Suzhou 215006, China
[c] Blackett Laboratory, Imperial College London, Prince Consort Road, London SW7 2BZ, United Kingdom
[d] Instituto de Estructura de la Materia (IEM-CSIC), Consejo Superior de Investigaciones Cientificas, Serrano 121, 28006 Madrid, Spain
[e] Nanoinstitute Munich, Faculty of Physics, Ludwig-Maximilians-Universität München, 80799 München, Germany

ARTICLE INFO

Keywords:
Hot electrons
Photoconversion
Thermodynamic losses

ABSTRACT

There are currently extensive interests on the hot-electron-mediated photoconversion. However, the device quantum yield is fundamentally low due to the existences of various hot-electron loss channels; moreover, the nanostructured plasmonic/metamaterial are generally required, which bring challenges to the low-cost and large-scale fabrication. In this study, we focus on distinguishing the thermodynamic losses in hot-electron devices and presenting the possible route-maps for performance improvement. It is shown that a number of optical, electrical, and material factors, which lead to the substantial losses of hot electrons during the generation, transport, and emission processes. These loss mechanisms involve extensively the photon absorption, resistive dissipation, electron/electron or electron/phonon thermalization, carrier diffusion, Schottky barrier, and electron-momentum conservation. We further exemplify several planar hot-electron systems to show the possibilities of breaking these limitations for high efficiency. The planar hot-electron devices are based on Tamm plasmons, microcavity with double barriers, and optimized system by controlling the barrier and electron density of state, respectively. Results indicate that these designs can significantly improve the efficiencies of hot-electron generation, transport, and collection. It reveals that the external quantum efficiency of the system after the multi-domain optimization can be up to 60% in the near-infrared band. This study will motivate deeper understanding on the physical mechanisms, which restrict the performance of hot-electron device, and provide the solutions to improve the performance of hot-electron devices.

1. Introduction

The generation of hot electrons in metal through nonradiative decay of plasmons offers new and exciting opportunities in directly converting light into electricity by forming a metal-semiconductor (M/S) Schottky junction [1–4], which enables the below-bandgap infrared photodetection with many advantages (such as convenient fabrication, room-temperature operation without electric bias, and high tunabilities of the working wavelength, *etc.*) [5–7]. To promote the hot-electron generation, metallic nanostructures that excite surface plasmons to concentrate the light within a subwavelength volume have been extensively demonstrated [8–12]. With plasmonic gratings, the photon energy can be strongly coupled into surface plasmons, resulting in a strong/narrowband absorption and intensive hot-electron generation proximal to the interfacial region. Such a system exhibits a photoresponsivity of 0.6 mA/W and an internal quantum efficiency (IQE) of ~0.2%, which is indeed not very high, but has already been improved by 20 times over the nanoantenna-based devices [6]. Further performance improvement can be realized by using metamaterial, where the hot electrons are efficiently generated within (for example) the 15 nm gold film, which is thin enough to ensure an effective electron transport to the interface and the resultant high photoresponsivity up to 3.37 mA/W [7]. Besides the widely discussed surface plasmons, other photonic mechanisms have also been considered recently for hot-

☆ The authors declare no competing financial interest.

* Corresponding author at: School of Optoelectronic Science and Engineering & Collaborative Innovation Center of Suzhou Nano Science and Technology, Soochow University, Suzhou 215006, China.
E-mail address: xfli@suda.edu.cn (X. Li).

https://doi.org/10.1016/j.nanoen.2018.10.051
Received 19 September 2018; Received in revised form 23 October 2018; Accepted 24 October 2018
Available online 31 October 2018
2211-2855/

electron photoconversion. For example, microcavity resonance [13,14] and Tamm plasmons [15] have been found highly beneficial for this kind of application under planar and low-cost system scenarios compared to conventional plasmonic systems with high-dimension and subwavelength nanopatterns.

Despite the enormous efforts, the photoconversion efficiencies of hot-electron devices are still low, preventing from their practical applications [16–18]. The previous studies primarily focused on the optical modulation for a higher-efficiency of hot-electron generation. However, the hot-electron devices involve complex optoelectronic process, where the device performance relies on both the optical and electrical properties. Particularly, some fundamental mechanisms during the generation, transport, and collection processes of hot-electron set the key limitations on the performance improvement of hot-electron devices, which cannot be solved by solely the optical methods. Therefore, a complete exploitation on the lossy mechanisms in hot-electron devices from the optical and electrical perspectives is highly beneficial from both fundamental science and the advanced optoelectronic applications.

To explore the possible ways to realize high-efficiency hot-electron photoconversion, we systematically address in this study the thermodynamic losses of hot electrons during the generation, transport, and collection processes. We suggest that 1) the lack of absorption, 2) the resistive dissipation from collective oscillation of electrons, 3) the nearly uniform hot-electron energy distribution, 4) the rapid thermalization due to electron-electron/electron-phonon scatterings, and 5) the momentum conservation in interfacial electron transfer are the primary and fundamental reasons for the extremely low hot-electron photoconversion efficiency. These mechanisms are discussed in detail with the exemplified strategies to break these limitations. For example, we indicate that the advances in the manipulation of light in metallic nanostructures, the modification of the Schottky interfaces, and the engineering of electron density of state (EDOS) in metallic materials can minimize the thermodynamic losses to obtain ultrahigh-efficiency hot-electron devices. Taking Au/Si barrier as an example, the external quantum efficiencies (EQE) of the thick-film single-barrier, thin-film single-barrier, and thin-film double-barrier configurations in the near-infrared region show extremely high EQE up to ~60%. Two planar hot-electron devices based on Tamm plasmons and microcavity are proposed to approach the efficiency limits. We show how the limiting factors such as the electron-momentum conservation, barrier height, and thermalization loss can be controlled by managing the light and hot electrons. This study is beneficial for deeply understanding the inherent science of hot-electron devices as well as motivating advanced solutions to overcome the fundamental limitations to obtain unprecedently high hot-electron photoconversion efficiency.

2. Result and discussion

2.1. Thermodynamics in hot-electron conversion

The approach addressing the various loss mechanisms for the hot-electron photoconversion as well as the opportunities for efficiency improvement is under the assumption that each plasmon by photon excitation decays into one energetic electron-hole pair, *i.e.*, high-order processes such as multiple electron-hole pair generation are forbidden [19,20]. Hot electrons are generated by an event of photon absorption (A), and each absorbed photon with energy E_{ph} raises only one electron from the occupied energy level below the Fermi level to the unoccupied high-energy level in the conduction band. Apart from the hot-electron generation via single-particle excitation, another source of the plasmon loss in metal is the classical resistive dissipation, as shown in Fig. 1a, where the *ab initio* predicted efficiency (η) of plasmons decay into hot electrons (η_{eh}) or dissipate thermally (η_{res}) in bulk gold as a function of plasmon energy is illustrated [19]. It is shown that the proportion of the resistive dissipation is increased under low-energy (long-wavelength) photon excitation.

After excitation, hot electrons are thermalized by the electron-electron and electron-phonon scatterings in tens of femtoseconds (10–100 fs), subsequently cooled by the energy transfer to the lattice in around 100 fs to 1 ps via electron-phonon scattering, and ultimately the lattice phonons are equilibrated with the surrounding bath on the timescale of 100 ps [21]. Under room temperature, the lifetimes of the electron-electron scattering, electron-phonon scattering, and phonon-phonon/bath thermalization are ~40 fs, 800 fs, and 86 ps, respectively (please see details for the effect of the temperature in the section S5 of Supporting Information). Only the electrons generated within the region defined by the mean free path (l_{MFP}) from the Schottky interface can participate effectively in interfacial electron transfer without encountering essential relaxation [22]. Fig. 1b shows the electron lifetime (τ) and l_{MFP} as a function of the electron excess energy above Fermi level (E_{ex}) in gold. The low-energy electrons have a long τ and a large l_{MFP} because the electron-phonon scattering dominates and the electron-electron scattering is negligible. Typically, in gold, hot electrons with $E_{ex} \sim 0.75$ eV have $l_{MFP} \sim 25$ nm and are thermalized within 14 fs.

For hot electrons arriving at the Schottky interface, only those with kinetic energy with the normal momentum component higher than the barrier height (φ_{SB}) can be injected into semiconductors [23]. However, even for the electrons diffusing perpendicularly to the interface, the proportion of the injected electrons with $E_{ex} > \varphi_{SB}$ is still low. For example, it is ~23% for incident photons with $\lambda = 1300$ nm in the Au/Si contact ($\varphi_{SB} = 0.75$ eV), calculated from the initial energy distribution, $D(E)$, of the excited hot electrons in the bottom panel of Fig. 1b. Due to the conservation of electron momentum component parallel to the Au/Si interface as shown in Fig. 1c, only a small fraction (η_{esc}) of electrons can accomplish the interfacial electron transfer process. Further considering the possible electron reflection at the interface due to the impedance mismatch, the proportion (η_{inj}) tends to be less [24], *e.g.*, $\eta_{inj} = 0.12$ even when $E_{ex} = 2\varphi_{SB}$.

From the above thermodynamic analysis of the hot-electron conversion process based on the three-step phenomenological model proposed by C. Scales and P. Berini by further adding additional physics to model the resistive dissipation in the hot-electron generation process, the thermalization loss in the hot-electron transport process, and the electron reflections at the M/S interface in the hot-electron collection process [23], the EQE of the hot-electron devices can be calculated by:

$$\mathrm{EQE}(\lambda) = A\eta_{eh}(\lambda) \times \int_{\varphi_{SB}}^{\infty} D(\lambda, E)\eta_{etr}(E) \times \eta_{inj}(E)dE \quad (1)$$

where λ is the wavelength, A the light absorption efficiency, η_{eh} the efficiency of plasmons decay into hot electrons, D the initial energy distribution, and η_{etr} (η_{inj}) hot-electron transport (injection) efficiency to Schottky interface (into semiconductors). It is obvious that the EQE value is determined by the five terms on the right under distinguished physical origins.

2.2. Categorized hot-electron losses

Based on the above analysis, we can categorize the mechanisms of hot-electron energy losses into three kinds occurring in the hot-electron generation, transport, and emission processes, respectively, and accordingly present the inherent physical limiting factors as well as provide the potential solutions (see Fig. 2).

2.2.1. Limitation 1: optical loss and resistive dissipation in hot-electron generation (I and II in Fig. 2)

Due to the significant impedance-mismatch between metal and air, there is a high reflectance by the planar metal surface, leading to very poor hot-electron generation. Therefore, the outstanding light-trapping strategy is of prominent importance to enhance the photoemission of hot electrons. This has been paid by the most past attention in the hot-electron photoconversion field. Considering that the plasmonic or metamaterial nanostructures have large absorption cross-sections and

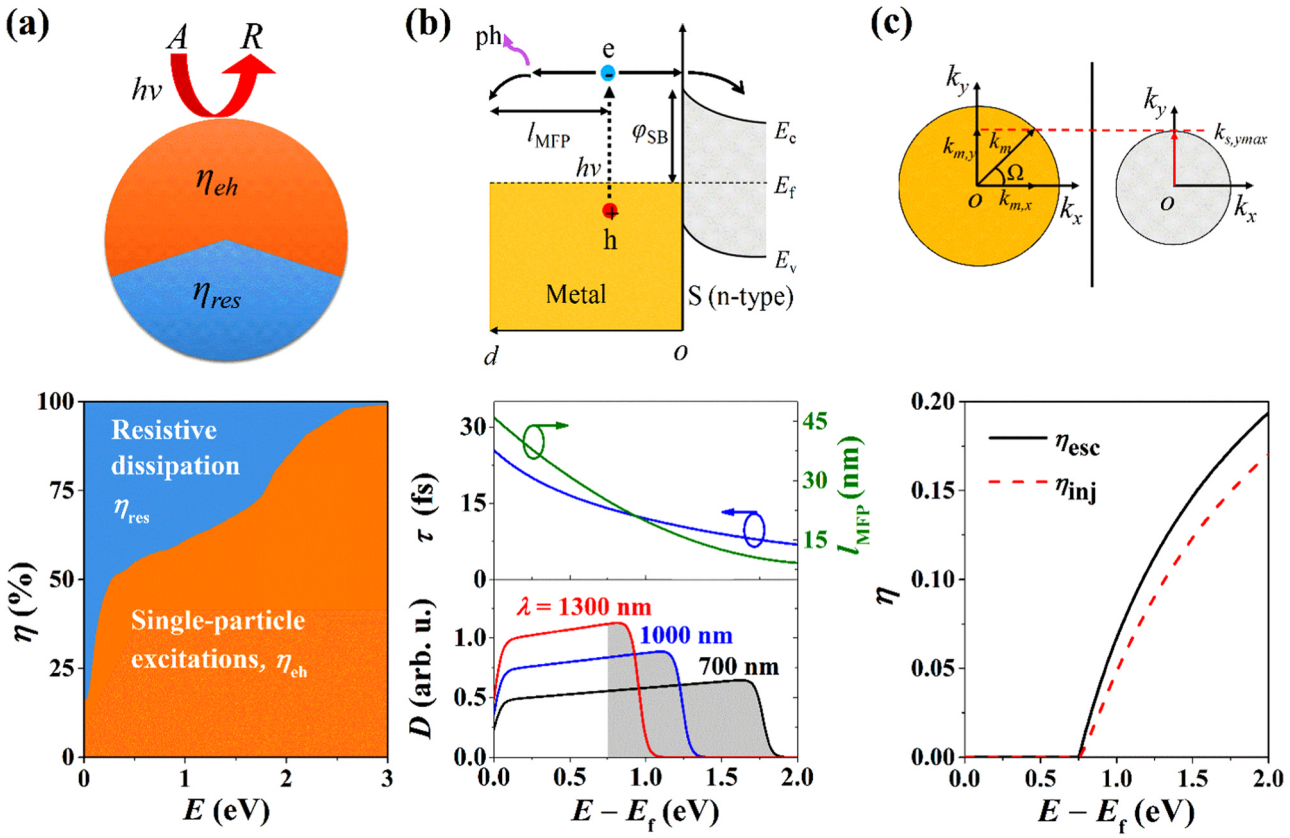

Fig. 1. The fundamental hot-electron photoconversion processes. (a) hot-electron generation, (b) transport and (c) injection into semiconductors. The external quantum efficiency (EQE) consists of the absorption efficiency (*A*), the efficiency of plasmons decay into hot electrons (η_{eh}), the efficiency of hot-electron transport to the interface (η_{etr}), and the efficiency of interfacial electron transfer into semiconductors (η_{inj}). The top panels show the schematic of (a) absorption, (b) thermalization mechanism, and (c) momentum conservation at each stage. The bottom panels show (a) the efficiency of η_{eh} and resistive dissipation (η_{res}) in bulk gold as a function of plasmon energy, (b) the hot carrier lifetimes, mean free paths & initial energy distribution of hot electrons, and (c) the collection efficiency of electrons at the interface without (with) the consideration of electron reflection η_{esc} (η_{inj}).

	Problem	Solution
Emission	(VI) Energy loss due to electron-momentum conservation	Thin-film, three-dimensional Schottky barrier
	(V) Energy loss due to Schottky barrier limit	Low barrier height, electron density of state engineering
Transport	(IV) Energy loss due to half of electrons diffusing away from Schottky interface	Double-barrier, external bias, initial electron-momentum distribution engineering
	(III) Energy loss due to electron-electron and electron-phonon thermalization	Electric field concentration near junction, thin-film
Generation	(II) Classical resistive dissipation due to collective oscillation of electrons	Small nanoparticles
	(I) Incomplete photon absorption	Light management

Fig. 2. Thermodynamic losses and solutions in hot-electron conversion. Energy losses in the hot-electron generation, transport and emission processes. The corresponding solutions are listed in the right column.

strongly enhanced electric fields in resonance, these artificially designed nanosystems have been discussed extensively as the efficient light-management strategies to improve the optical absorption for efficient hot-electron generation [25]. Apart from the optical loss, the short-lived electronic states comprising the collective oscillation leads to the classic resistive loss with energies converted into heat. The resistive contribution to plasmon loss in metal is expected to reduce with lowering the temperature. Below the interband threshold, resistive loss competes with phonon-assisted excitations and accounts for ~30%–50% of the absorbed energy [19]. Fortunately, the proportion of resistive loss (η_{res}) in the metallic absorption can be reduced by using smaller gold nanoparticles [19], *e.g.*, η_{eh} is improved to ~90% in a 10 nm-diameter sphere from 60% in bulk gold with E_{ph} = 1 eV [19].

2.2.2. *Limitation 2: thermalization loss in hot-electron transport (III and IV in Fig. 2)*

The first step for hot-electron transport is the diffusion from the position of hot-electron generation to the M/S interface, which is mostly determined by the mean free path of hot electrons and the diffusion angle (see Equation S5 of the Supporting information). However, it has been indicated that only a small fraction of hot electrons can reach the interface due to the rapid relaxation [23]. To improve the hot-electron transport efficiency, concentrating the electric field near M/S interface or employing a metal film with a thickness smaller than l_{MFP} are promising ways [26,27]. For the conventional single-barrier Schottky device, half of hot electrons will transport toward the M/S interface based on the assumption of isotropic initial momentum distribution [23]. Technically, this can be solved by modifying the initial momentum distribution of hot electrons by engineering the surface plasmon mode since hot electrons are preferentially generated with a momentum parallel to the electric field [20]. By the excitation of surface plasmon under TM illumination, more electric fields lie in the direction normal to M/S interface compared to that under TE case (purely tangential to M/S interface). The hot electrons are initially generated with a *k*-vector matching the plasmon mode by the Landau damping and preferentially directed along the surface plasmon momentum direction [24]. For example, applying an external electric bias facilitates the unidirectional hot-electron transport toward the interface [28].

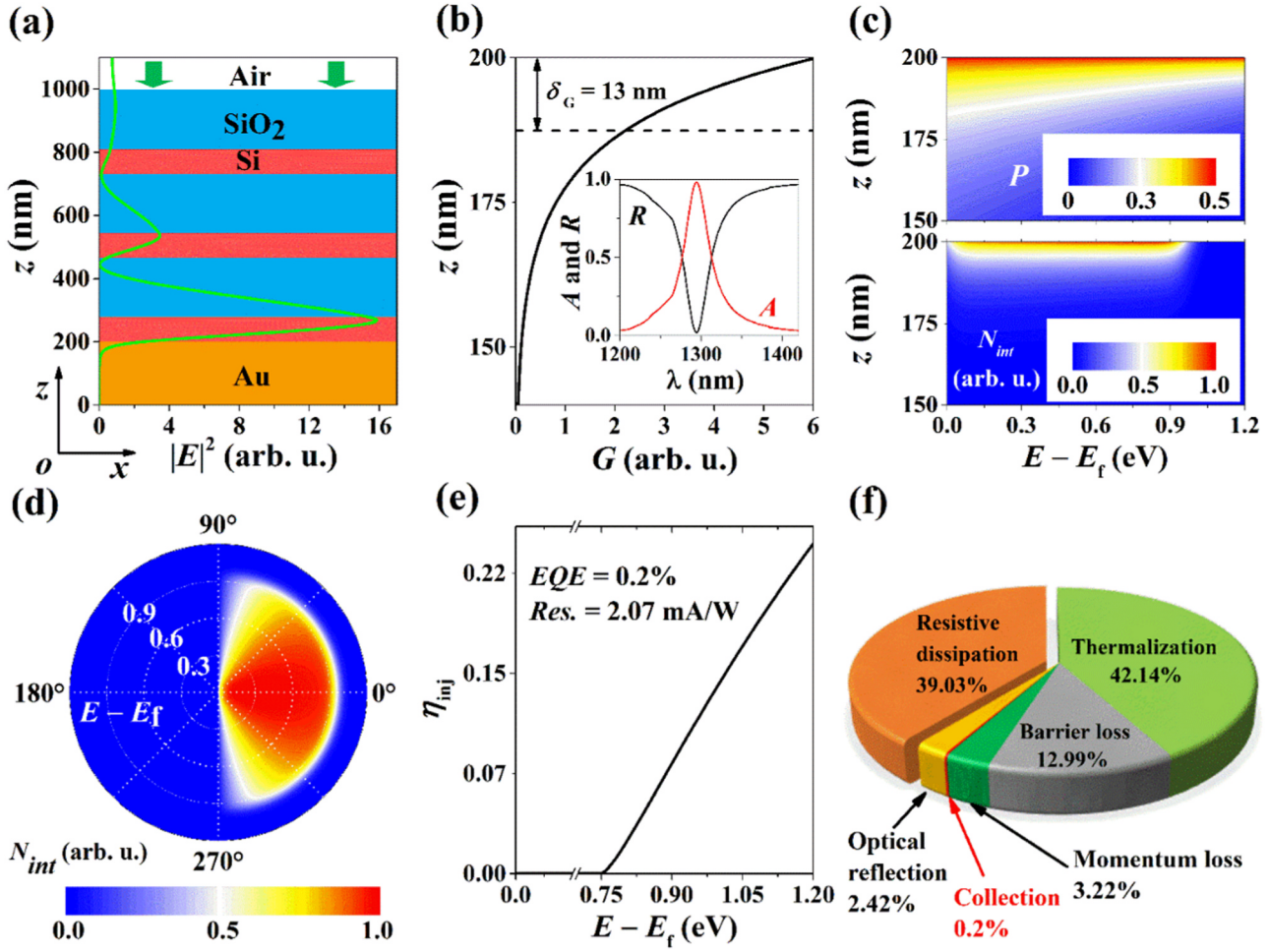

Fig. 3. Device I and optoelectronic performance. (a) Schematic diagram of the proposed TP-induced hot-electron system with the profile of the normalized electric field at TP wavelength. (b) Profile of the hot-electron generation along *z*-axis with optical response of the device inserted. The contour map of (top panel in c) the probability and the flux of electrons with energy *E* that reach the M/S interface (bottom panel in c) at position *z* and (d) under an angle *θ*. (e) Emission probability of electrons into semiconductors with the consideration of electron reflections at interface. (f) Energy collection and loss distribution in Device I.

Furthermore, employing double Schottky barriers is an effective strategy since all of the hot electrons will diffuse toward the M/S interfaces now.

2.2.3. Limitation 3: low collection efficiency in hot-electron emission process (V and VI in Fig. 2)

The other fundamental restriction for the efficient hot-electron collection is the Schottky barrier height, which hinders the low-energy electrons from emission into semiconductors. Thus, a low barrier height is generally preferred. Recent studies have shown that the barrier height can be strongly affected by the details of the interface, which may vary significantly with the fabrication method and surface treatment [16,18]. Another strategy is to engineer the EDOS with the band edge just below the Fermi level, which results in a narrow energy distribution with a single peak above the barrier height [12,18,29]. Since only the electrons within the escape cone of momentum space have a relatively high probability to transport across the interface, the injection probability is expected to be boosted with a thin metal film due to multiple electron reflections between the internal metal surfaces [23]. Another approach to overcome the momentum limitation of electron emission over the barrier is to form a three dimensional (3D) Schottky barrier by embedding the plasmonic nanostructure within the semiconductor [30]. The Schottky barriers formed on the vertical sides of the metal in addition to the planar Schottky interface increase the momentum space for hot-electron emission. Moreover, the electric field is strongly localized in the metallic grating edges, where more hot electrons are generated. The abrupt boundaries provide the necessary momentum for electrons to inject into semiconductor and relax the requirement of the parallel momentum conservation [24]. Besides, roughening the M/S surface can relieve the momentum restriction by providing the necessary tangential momentum for the carrier injection [24,31,32]. This analysis could be highly desirable for understanding the limiting factors and providing potential solutions for the efficient conversion of hot electrons. In the following sections, we will show the role of light and carrier management in improving the efficiency using Au/Si barrier as an example. It is noted that the discussed strategies are universal and applicable to other hot-electron systems.

2.3. Solutions for improved efficiency

Above analyses indicate that there are various loss mechanisms during the generation, transport, and collection processes, resulting in the low hot-electron photoconversion efficiency. Our categorized investigation allows exploring the corresponding solution for each limiting factor so that the device performance can be improved step-by-step. In the following, we will introduce three kinds of designs, each of which solves a specific problem in the hot-electron generation, transport, or collection process. It is noted that the methods/strategies presented here are general and applicable for the systems with other metals and semiconductors.

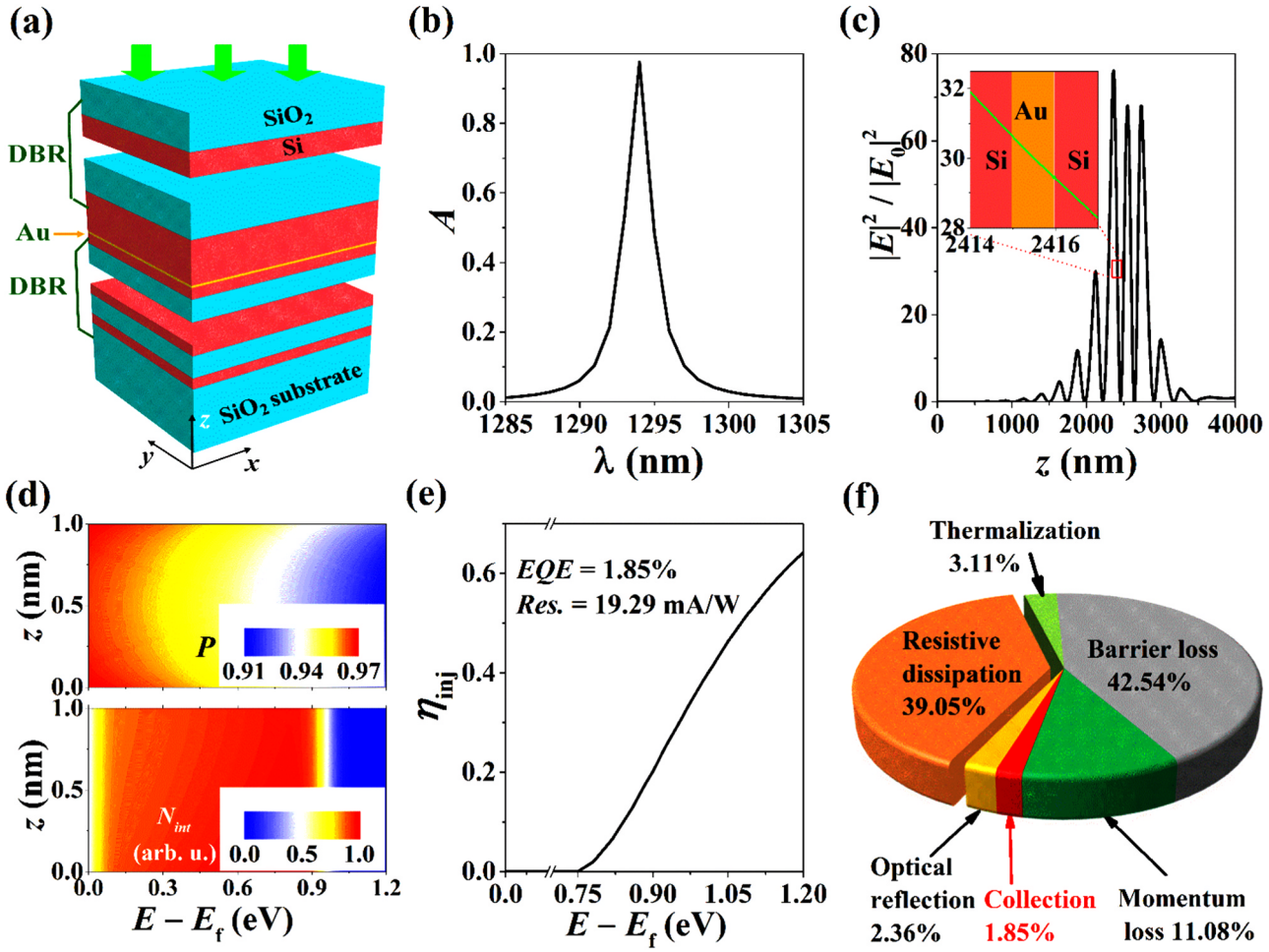

Fig. 4. Device II and optoelectronic performance. (a) Schematic diagram of the ultrathin-film double-barrier hot-electron device. (b) Absorption spectrum of the device. (c) Electric field profile along *z*-axis. Enlarged figure shows the electric field in the Au zone. The contour map of (top panel in d) the probability and (bottom panel in d) the flux of electrons with energy *E* that reach MS interface at position *z*. (e) Emission probability of electrons in the ultrathin-film double-barrier device. (f) Energy collection and loss distribution in Device II.

2.4. Hot-electron generation engineering

The first example is shown to obtain the significantly improved optical absorption by the planar multilayer design. The system (*i.e.*, Device I) is composed of three pairs of alternating SiO_2/Si (each with the quarter-wavelength thickness) on an Au layer with the thickness d_{Au} = 200 nm, as shown in Fig. 3a. The refractive index of Si is taken as 3.5 for the design of distributed Bragger reflector (DBR) with the central wavelength λ_{DBR} = 1100 nm. The Si layer in contact with Au is n-type doped, forming a single Schottky barrier. Tamm plasmons (TPs) are excited in the system with light propagating along the DBR/Au boundary [15], thus the electric field is highly confined in the region and decays exponentially toward the Au layer (see Fig. 3a), resulting in a narrow reflection dip and perfect absorption on resonance (see the inset of Fig. 3b). As a result, most hot electrons are generated close to the upper surface of the metal film with δ_G = 13 nm, which is defined as the distance where the generation rate drops to $1/e$ of the maximum (see Fig. 3b). Even for the excited highest-energy electrons, δ_G is smaller than l_{MFP} (18 nm), which implies a favorable hot-electron spatial distribution with a relatively large probability to reach the interface (see the top panel of Fig. 3c). Most hot electrons reaching the interface come from that generated in the region close to the upper surface of Au due to the high generation rate and transport probability there (see the bottom panel of Fig. 3c). The overall hot-electron transport efficiency η_{trans} (defined by Equation S8 in the Supporting information) is 28%, which is 11.6 times larger than the value of 2.4% for plasmonic nanostripe-based device [24].

The angular distribution of ballistic electrons reaching the interface is quite anisotropic since under a larger diffusing angle, the propagation path is increased and more electrons will be thermalized (see Fig. 3d). With the injection efficiency of electrons reaching the interface (see Fig. 3e), the EQE and the responsivity of the device are obtained as 0.2% and 2.07 mA/W, respectively, which are more than 3 times of those based on plasmonic nanograting [6]. Besides, the IQE ~ 0.2% (under $A \sim 1$) of the device is the same as that of the grating nanostructure, which further demonstrates that an efficient optical absorption is vital to the high-performance hot-electron device. For a further insight into the energy losses, we compare the various contributions of the energy losses by examining the hot-electron flux at each stage in Fig. 3f. It is found that the resistive dissipation and thermalization

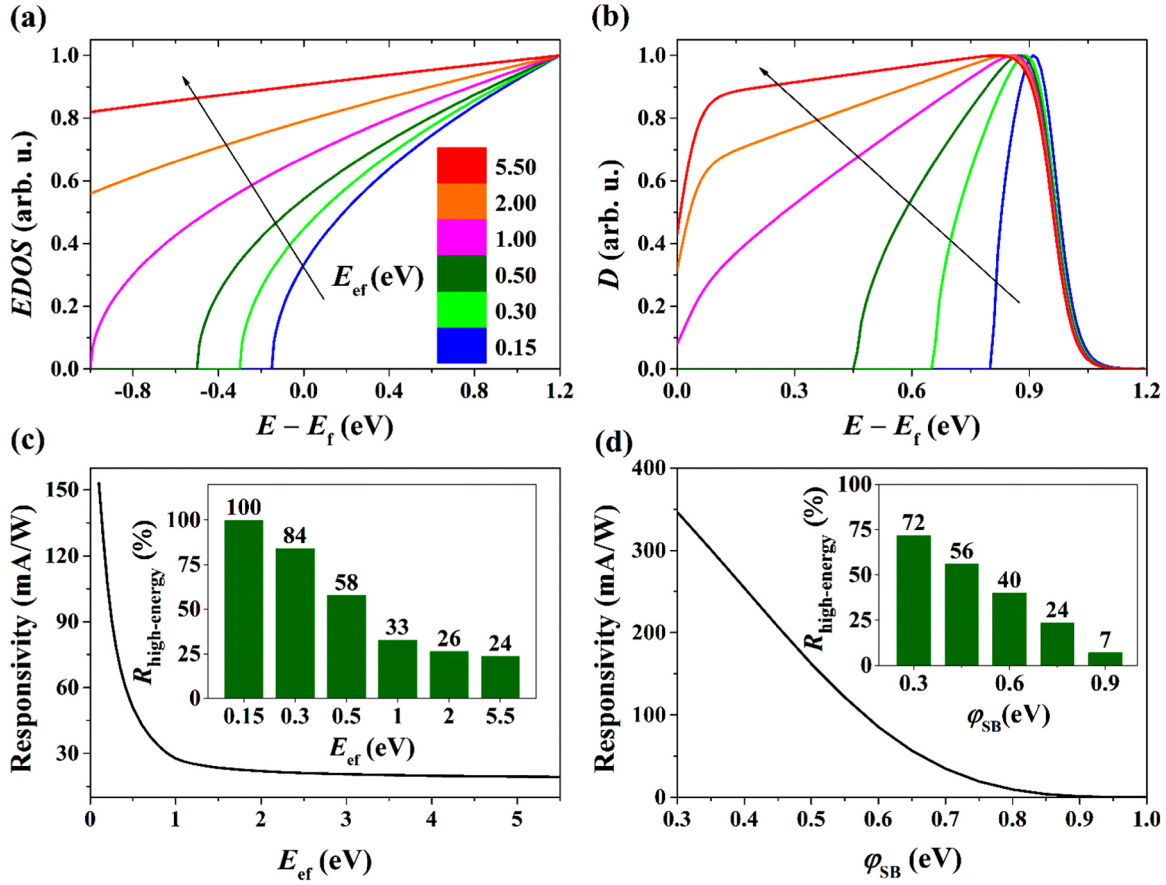

Fig. 5. Optimization on EDOS and barrier. Further improving the conversion efficiency in the ultrathin-film double-barrier hot-electron device by engineering the EDOS and the barrier height. (a) Ideal parabolic EDOS with the effective Fermi level (E_{ef}) ranging from 0.15 to 5.5 eV. (b) The corresponding initial energy distribution of hot electrons within a narrow energy range for low E_{ef}. (c, d) the responsivity as a function of E_{ef} and φ_{SB}, respectively, where the fraction of over-barrier hot electrons are inserted.

losses dominate the energy losses in the device. In contrary, the collected energy in the system is negligible, showing the great chance for the development of ultrahigh-efficiency hot-electron device. The barrier loss is higher than the sum of the optical reflection and momentum loss.

2.5. Hot-electron transport engineering

In hot-electron devices, the electron diffusion is normally uncontrolled if not any external means employed; therefore, only half of the hot electrons diffuse toward the Schottky interface in the single-barrier systems. To conquer this limitation, an ultrathin-film double-barrier system (Device II) is proposed in this study (see Fig. 4a). The double Schottky junctions can be formed by burying the 1 nm Au film into a Si layer, which are covered by two DBRs. We performed the optical optimization on the top and bottom DBRs in order to obtain the highest optical absorption. Specifically, the top DBR is consisted of 3.5 pairs of SiO_2/Si (thickness of 150/113 nm) on top of a 330 nm Si buffer layer and the bottom DBR has 10 pairs of SiO_2/Si (thickness of 71.4/170 nm). The special design enables a perfect absorption (see Fig. 4b) and ~30-fold enhancement of the local electric field in Au film (see Fig. 4c) at the same resonance of Device I under normal incidence. The ultrathin metal film leads to an extremely high hot-electron transport probability (see the top panel of Fig. 4d), uniform spatial distribution of electrons reaching the interface (see the bottom panel of Fig. 4d), and nearly isotropic momentum distribution of electrons at the interface (not shown here). Fig. 4e indicates that the injection efficiency of the electrons into the semiconductor is more than twice of that in Device I, due to the emission over two barriers and multiple electron reflections between the double Au/Si interfaces. As a result, the responsivity (EQE) of Device II is 19.29 mA/W (1.85%), which is the highest value reported in the hot-electron systems. However, it is still much lower than that in the hot-hole device with PtSi/p-Si arising from the smaller Schottky barrier height [33,34]. It is clear from Fig. 4f that the thermalization loss is decreased dramatically, while the barrier and momentum losses are increased since there are more electrons reaching the interface.

2.6. Hot-electron collection engineering

With the above improvements on the optical absorption and electrical diffusion, the further strategy to promote the system performance is to optimize the hot-electron collection by controlling the barrier configuration or the hot-electron momentum direction. Here we examine the opportunity to further improve the photoresponsivity of Device II by promoting the ratio ($R_{high\text{-}energy}$) of over-barrier hot electrons within the overall excitation. Figs. 5a and 5b show the parabolic EDOS and the resulting hot-electron distribution with raising the effective Fermi level E_{ef} from 0.15 to 5.5 eV (E_{ef}: the effective conduction bandadge below the Fermi level of the metal [12,18,29]). With a lower E_{ef}, more electrons are concentrated within an extremely narrow energy range below Fermi level at thermal equilibrium. The excited hot

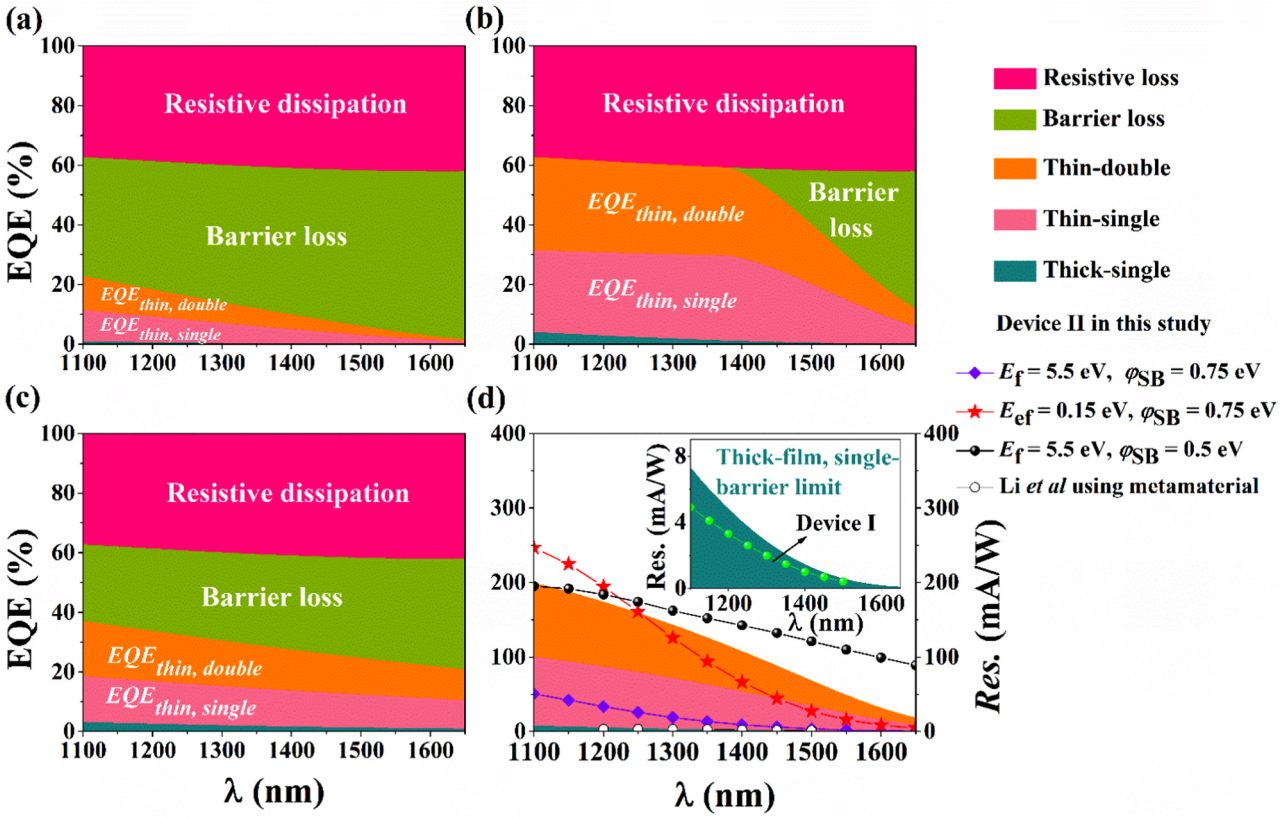

Fig. 6. EQE limits of planar hot-electron devices. Wavelength-dependent limiting EQE of the planar hot-electron device for (a) E_{ef} = 5.5 eV & φ_{SB} = 0.75 eV, (b) E_{ef} = 0.15 eV & φ_{SB} = 0.75 eV, and (c) E_f = 5.5 eV & φ_{SB} = 0.5 eV. (d) Limiting responsivity spectra of the thick-film single-barrier, thin-film single-barrier, and thin-film double-barrier hot-electron devices, where the responsivity of the realistic device (Device II) with E_f and φ_{SB} from Figures 6a–6c are inserted for comparison. The spectrum of the limiting responsivity for the thick-film single-barrier hot-electron device is enlarged in the inset, to compare with the responsivity of Device I. (For interpretation of the references to color in this figure, the reader is referred to the web version of this article).

electrons are distributed in a higher and narrower energy range, which results in an increased $R_{high\text{-}energy}$ (see the inset of Fig. 5c), *e.g.*, all excited electrons have enough energy to overcome the barrier ($R_{high\text{-}energy}$ = 100%) at E_{ef} = 0.15 eV. On contrary, with a high E_{ef}, a number of electrons are located away from the Fermi level and the hot-electron distribution is broad and nearly uniform (i.e., the significantly decreased $R_{high\text{-}energy}$), which is detrimental to hot-electron collection. As a result, the responsivity is increased from 27.7 to 152.9 mA/W with lowering E_{ef} from 1 to 0.1 eV (see Fig. 5c). Moreover, the responsivity of the hot-electron device can also be improved by using a lower barrier height, which directly leads to an increased $R_{high\text{-}energy}$ and allows more electrons to accomplish the interfacial electron transfer process (see Fig. 5d). However, it is worth to note that the lower barrier height dramatically increases the thermal emission and results in a higher dark current, so the tradeoff must be considered to maximize the overall photocurrent.

2.7. Efficiency limit of hot-electron devices

We now show the potential route-maps for the hot-electron device to improve the efficiency. The limiting EQEs of the planar hot-electron devices under various configurations, including thick-film, thin-film, single-barrier, and double-barrier, are examined and compared. Here, we list the strategies to enhance the device performance step-by-step. 1) For thick-film single-barrier device, the perfect hot-electron transport denotes the limiting η_{trans} = 0.5 (*i.e.*, all of the hot electrons are distributed in the region very close to the interface), allowing to obtain the corresponding limiting EQE. 2) With a thin-film configuration, the hot-electron collection efficiency η_{inj} can be further improved. Ideally, for the over-barrier hot electrons, we have η_{inj} = 1 if $E_{ex} > \varphi_{SB}$; therefore, the corresponding EQE limit of thin-film single-barrier device can be achieved. 3) Actually, the highest η_{trans} = 0.5 in single-barrier system can be further improved up to 1 by employing the double-barrier, leading to the doubled limiting EQE compared to the single-barrier system. 4) In addition, if all excited hot electrons can be collected by engineering the EDOS of the metal, the barrier loss can be completely suppressed, enabling even higher EQE. 5) Finally, neglecting the resistive loss of the absorbed energy in the small metallic nanoparticles, the perfect conversion with EQE = 100% can be obtained in principle, *i.e.*, all incident energy can be converted into photocurrent.

Figure 6a – c plot the spectra of limiting EQE of the planar hot-electron devices under thick-film single-barrier, thin-film single-barrier, and thin-film double-barrier configurations. Moreover, the possible EQE spectra with eliminating the barrier and resistive losses are introduced into the optimized system in order to examine the upper-limit of the EQE. In these three figures, the distinguished electrical parameters are also considered, i.e., (a) E_{ef} = 5.5 eV and φ_{SB} = 0.75 eV, (b) E_{ef} = 0.15 eV and φ_{SB} = 0.75 eV, and (c) E_{ef} = 5.5 eV and φ_{SB} = 0.5 eV. The contribution of the wavelength-dependent resistive loss to absorption in metal is taken from Ref. [19]. It is found that, even for the ideal planar thick-film/single-barrier hot-electron device, the EQE is extremely low, leaving a great room for improvement by increasing the

interfacial electron injection efficiency with a thin-film metal and collecting more electrons with double Schottky junctions. With a very low $E_{ef} = 0.15$ eV (Fig. 6b), the barrier loss is eliminated when $\lambda < 1377$ nm because all excited hot electrons have energies higher than φ_{SB}. In this case, the momentum and thermalization losses are the main limiting factors, so the thin-film double-barrier setup can be used for a high conversion efficiency. With a low barrier height (Fig. 6c), the barrier loss is slightly relieved and the sum of thermalization and the momentum losses tends to compete with that of the barrier loss.

The corresponding responsivity spectra of the thick-film single-barrier, thin-film single-barrier, and thin-film double-barrier hot-electron devices shown in Fig. 6a are plotted in Fig. 6d, where the responsivity spectra of i) an actual system (*i.e.*, Device II) with E_{ef} and φ_{SB} corresponding to Figure 6a−c and ii) a metamaterial system are included. It is shown that the responsivity of Device II with $E_{ef} = 5.5$ eV and $\varphi_{SB} = 0.75$ eV can be even one-magnitude larger than the highest reported value in the hot-electron device by integrating the metamaterial perfect absorber as marked by the white circles [7]. The engineering of EDOS (redline with star-marker) and barrier height (blackline with sphere marker) can make the responsivity higher than the limiting values. It is noted that the responsivity of Device I is close to the theoretical limit of the thick-film single-barrier device, especially at long-wavelength band (see the inset of Fig. 6d). With the optimized optoelectronic design and properly modulating the values of E_{ef} and φ_{SB}, the responsivity of Device II exhibits the significantly increased responsivity, revealing the way to realize high-efficiency planar hot-electron devices.

It is noted that the EQE itself cannot reveal enough information of the device performance, so we discuss the effect of dark current here. The dark current density can be obtained from the thermionic emission theory [26]:

$$J_{dark}(T, V) = A^{**}T^2 e^{\frac{-q\varphi_{SB}}{k_B T}}\left(e^{\frac{qV}{k_B T}-1}\right) \quad (2)$$

where A^{**} is the effective Richardson constant, T is the operation temperature, k_B is the Boltzmann's constant, and V is the voltage across the device. With a low barrier height, the EQE is high, while the resulting large dark current may lead to a low conversion efficiency. Although the dark current is small for a high barrier height, the conversion efficiency may be low as well due to the decreased EQE. Reducing the operation temperature is an effective way to obtain a low dark current and a high conversion efficiency. However, cooling needs more energy consumption and is inconvenient, especially for an extremely low temperature. Thus, choosing a reasonable barrier height to balance the dark current and EQE is essential to obtain a high conversion efficiency. It is noted that the high EQE and responsivity of the hot-electron devices can be obtained without applying an external bias.

3. Conclusions

In summary, we systematically investigate the fundamental thermodynamic losses in the hot-electron generation, transport, and emission processes, elucidate the inherent physical limitations to the photoconversion efficiency, and highlight the opportunities for solving/relieving the problems. The low optical absorption, resistive dissipation, nearly uniform hot-electron energy distribution, rapid hot-electron thermalization, and momentum conservation in interfacial electron transfer are found to be the key reasons leading to the extremely low hot-electron photoconversion efficiency. Based on the analysis, we present a planar multilayer system composed of three pairs of DBR on metal with the excitation of TPs, which enables the perfect absorption and efficient hot-electron transport to the M/S interface. It is found that the responsivity can be as high as 2.07 mA/W, which is close to the theoretical limit of the thick-film single-barrier hot-electron devices. We further design an ultrathin-film double-barrier system which shows the perfect optical absorption, dramatically decreased thermalization loss, and improved injection probability, leading to an extremely high responsivity up to 19.29 mA/W (one-magnitude larger than the highest reported using metamaterial perfect absorber). Further, the low effective Fermi level can promote $R_{high\text{-}energy}$, allows more electrons to accomplish the interfacial electron transfer process, and results in a high responsivity up to 152.9 mA/W. By simulation, the optimized planar hot-electron devices under thin-film double-barrier design exhibits an EQE as high as 60% in the near-infrared region. The thermodynamic analysis on the fundamental science, the proposed potential solutions, and the planar devices with extremely high performance provide the communities the opportunities to realize high-efficiency and low-cost hot-electron devices.

Acknowledgements

This work is supported by National Natural Science Foundation of China (61675142, 61875143, and 61775154), the Academic Start-up Funding of Soochow University (GD15900118), Natural Science Research Project of Jiangsu Higher Education Institutions (17KJA480004), and Priority Academic Program Development (PAPD) of Jiangsu Higher Education Institutions.

Appendix A. Supporting information

Supplementary data associated with this article can be found in the online version at doi:10.1016/j.nanoen.2018.10.051.

References

[1] M.W. Knight, H. Sobhani, P. Nordlander, N.J. Halas, Science 332 (2011) 702–704.
[2] M.L. Brongersma, N.J. Halas, P. Nordlander, Nat. Nanotechnol. 10 (2015) 25–34.
[3] C. Clavero, Nat. Photon. 8 (2014) 95–103.
[4] M. Moskovits, Nat. Nanotechnol. 10 (2015) 6–8.
[5] W. Li, J.G. Valentine, Nanophotonics 6 (2017) 177–191.
[6] A. Sobhani, M.W. Knight, Y. Wang, B. Zheng, N.S. King, L.V. Brown, Z. Fang, P. Nordlander, N.J. Halas, Nat. Commun. 4 (2013) 1643.
[7] W. Li, J. Valentine, Nano Lett. 14 (2014) 3510–3514.
[8] K.-T. Lin, H.-L. Chen, Y.-S. Lai, C.-C. Yu, Nat. Commun. 5 (2014) 3288.
[9] F.P.G.D. Arquer, A. Mihi, G. Konstantatos, ACS Photon. 2 (2015) 950–957.
[10] C. Zhang, K. Wu, B. Ling, X. Li, J. Photonics Energy 6 (2016) 042502.
[11] K. Wu, Y. Zhan, C. Zhang, S. Wu, X. Li, Sci. Rep. 5 (2015) 14304.
[12] C. Ng, J.J. Cadusch, S. Dligatch, A. Roberts, T.J. Davis, P. Mulvaney, D.E. Gómez, ACS Nano 10 (2016) 4704–4711.
[13] Y. Zhan, K. Wu, C. Zhang, S. Wu, X. Li, Opt. Lett. 40 (2016) 4261–4264.
[14] C. Zhang, K. Wu, Y. Zhan, V. Giannini, X. Li, Nanoscale 8 (2016) 10323–10329.
[15] C. Zhang, K. Wu, V. Giannini, X. Li, ACS Nano 11 (2017) 1719–1727.
[16] T. Gong, J.N. Munday, Nano Lett. 15 (2014) 147–152.
[17] P. Narang, R. Sundararaman, H.A. Atwater, Nanophotonics 5 (2016) 96–111.
[18] T.P. White, K.R. Catchpole, Appl. Phys. Lett. 101 (2012) 073905.
[19] A.M. Brown, R. Sundararaman, P. Narang, W.A. Goddard III, H.A. Atwater, ACS Nano 10 (2017) 957–966.
[20] A. Manjavacas, J.G. Liu, V. Kulkarni, P. Nordlander, ACS Nano 8 (2014) 7630–7638.
[21] J.G. Smith, J.A. Faucheaux, P.K. Jain, Nano Today 10 (2015) 67–80.
[22] B.Y. Zheng, H. Zhao, A. Manjavacas, M. McClain, P. Nordlander, N.J. Halas, Nat. Commun. 6 (2015) 7797.
[23] C. Scales, P. Berini, IEEE J. Quantum Electron. 46 (2010) 633–643.
[24] H. Chalabi, D. Schoen, M.L. Brongersma, Nano Lett. 14 (2014) 1374–1380.
[25] A.O. Govorov, H. Zhang, H.V. Demir, Y.K. Gun'ko, Nano Today 9 (2014) 85–101.
[26] M. Sakhdari, M. Hajizadegan, M. Farhat, P.Y. Chen, Nano Energy 26 (2016) 371–381.
[27] F. Wang, N.A. Melosh, Nano Lett. 11 (2011) 5426–5430.
[28] J. Hou, H. Zhu, J.C. Reed, F. Yi, E. Cubukcu, D.A. Bonnell, Appl. Phys. Lett. 110 (2017) 043103.
[29] T. Gong, J.N. Munday, Opt. Mater. Express 5 (2015) 2501–2512.
[30] M.W. Knight, Y. Wang, A.S. Urban, A. Sobhani, B.Y. Zheng, P. Nordlander, N.J. Halas, Nano Lett. 13 (2013) 1687–1692.
[31] A.O. Govorov, H. Zhang, Y.K. Gun'ko, J. Phys. Chem. C 117 (2013) 16616–16631.
[32] V.E. Babicheva, S.V. Zhukovsky, R.S. Ikhsanov, I.E. Protsenko, I.V. Smetanin, A. Uskov, ACS Photon. 2 (2015) 1039–1048.
[33] W.F. Kosonocky, F.W. Shallcross, T.S. Villani, J.V. Groppe, IEEE Trans. Electron Device. 32 (1985) 1564–1573.
[34] C.K. Chen, B. Nechay, B.-Y. Tsaur, IEEE Trans. Electron Device. 38 (1991) 1094–1103.

Dr. Cheng Zhang received B.Eng. (2013) and Ph.D. (2018) degrees from Soochow University, China. He is currently working as an assistant professor in the School of Optoelectronic Science and Engineering, Soochow University, China. His research interests include the high-performance hot-carrier photodetection and the advanced light trapping designs for nanostructured solar cells. He has published around 10 1st author papers in journals including ACS Nano, Nano Energy, Nanoscale, Applied Physics Letters, Optics Letters, Nanoscale Research Letters, etc.

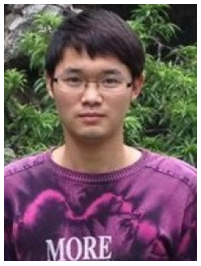

Guoyang Cao received his B.Eng. degree from Soochow University in 2014. He is now a Ph.D. student in the School of Optoelectronic Science and Engineering, Soochow University. His research interests include the advanced light trapping designs for nanostructured solar cells and optoelectronic simulation for the 2D-transition metal dichalcogenides-based photoconversion and photodetection devices. He has published 6 papers in Nano Energy, Optics Express, Applied Physics Letters, Solar RRL, Optics Letters, and Nanoscale Research Letters. Mr. Cao leaded a provincial research project, and won the National Scholarship for Postgraduate Students of China.

Prof. Shaolong Wu received the B.S. degree in Applied Physics from Nanchang University, China, in 2008, and the Ph.D. degree in Condensed Matter Physics from Beijing Normal University, China, in 2013. He is currently working as an associate professor in the School of Optoelectronic Science and Engineering, Soochow University, China. He has authored and co-authored more than 40 scientific articles. His current research interests focus on micro/nanostructure fabrication, solar energy conversion, and photon detection.

Dr. Weijia Shao received the B.S. degree in Applied Physics from Hefei University of Technology, China, in 2008, and the Ph.D. degree in Nuclear Science and Technology from University of Science and Technology of China, in 2014. He is currently working as a postdoctoral fellow in the School of Optoelectronic Science and Engineering, Soochow University, China. His current research interests focus on the simulation and calculation of solar energy conversion and photon detection.

Dr. Vincenzo Giannini started his scientific adventure as Physics undergraduate students at the University of Pisa. Later, he moved to Spain for a Ph.D. program at the Spanish research council (CSIC) in Madrid. He worked as a postdoc in Amsterdam and a Marie Curie fellowship at the Imperial College London after Madrid. In June 2014, he started his group at the Imperial College London in the Condensed Matter Theory section. He recently accepted an offer in Spain at the CSIC. His scientific interests rely on theoretical light-matter interactions, in particular, theoretical linear and nonlinear Plasmonics and Nanophotonics.

Prof. Stefan A. Maier holds the Chair in Hybrid Nanosystems at Ludwig-Maximilians-Universität München, and the Lee-Lucas Chair in Physics at Imperial College London. He is a fellow of the Optical Society of America and of the Institute of Physics.

Prof. Xiaofeng Li received B.Eng. (2002) and Ph.D. (2007) degrees from Southwest Jiaotong University, China, and has been working in Nanyang Technological University and Imperial College London for 5 years. Since 2012, he is working at Soochow University as a distinguished professor and currently serving as the dean of School of Optoelectronic Science and Engineering. His interests include photovoltaics, surface-plasmons, and advanced photoconversions, with ~ 120 journal publications and > 30 invited talks. He is senior member of IEEE and Optical Society of China, member of OSA and SPIE, Topical Editor of OSA Applied Optics, associate editor of IEEE Photonics Journal, and Editorial Board Member of Scientific Reports.